Supporting Information

Large-Area Monolayer Films of Hexagonal Close-Packed Au@Ag Nanoparticles as Substrates for SERS-based Quantitative Determination

Lixiang Xing,[a] *Yujiao Xiahou,*[a] *Xiang Zhang,*[a] *Wei Du,*[b] *Panpan Zhang*[*,c] *Haibing Xia*[*,a]

[a] State Key Laboratory of Crystal Materials, Shandong University, Jinan, 250100, P. R. China.

E-mail: hbxia@sdu.edu.cn

[b] School of Environment and Material Engineering, Yantai University, Yantai 264005, P. R. China.

[c] The Center of Esthetic Dentistry, Jinan Stomatological Hospital, Jinan 250001, China. No.101 Jingliu Rd, Jinan, P.R. China.

Experimental Section

Materials. Hydrogen tetrachloroaurate(III) tetrahydrate ($HAuCl_4 \cdot 4H_2O$), Trisodium citrate dihydrate ($Na_3C_6H_5O_7 \cdot 2H_2O$, 99 %), crystal violet ($C_{25}H_{30}N_3Cl$), ascorbic acid (AA, 99.7%), ammonia water ($NH_3 \cdot H_2O$, 25%～28%), toluene (C_7H_8), and ethanol absolute (C_2H_6O, 99.7 %) were purchased from Sinopharm Chemical Reagent Co. Ltd. Silver nitrate ($AgNO_3$, 99.995%) and 4-aminothiophenol (C_6H_7NS) were purchased from Alfa Aesar (China). Oleylamine ($C_{18}H_{37}N$) and diethylene glycol ($C_4H_{10}O_3$, 98 %) were purchased from Aladdin Industrial Co. Ltd and Shanghai Titan Scientific Co. Ltd, respectively. Polydimethylsiloxane (PDMS) was purchased from Dow Corning (Shanghai) Co. Ltd. All chemicals were used as received without further purification. The Milli-Q water was used in all experiments (18 MΩ cm, Millipore).

Fabrication of LAMF-HCP-Au@Ag NPs. The amount of the NPs used for self-assembly is calculated according to the following formula (1):

$$N = \frac{\pi * R^2}{\pi * r^2} = \frac{R^2}{r^2} \qquad (1)$$

It is assumed that all of the NPs are closely packed in a monolayer on the surface of the DEG phase. R and r are the radius of spherical interface area for assembly (inner radius of the culture dish in our case) and the radius of spherical NPs, respectively.

In our case, the interface area for NP assembly is equal to the inner surface area of the culture dish with an inner diameter of 7 cm. Taking the assembly of OLA-$Au_{5.5}$@$Ag_{5.25}$ NPs as an example, its concentration of particle number (C_{NUM}) in the toluene phase after the phase transfer is calculated to be 4.9×10^{12} mL^{-1}, since the volume ratio of the aqueous solution of

citrate-stabilized Au@Ag NPs (9.8×10^{11} mL^{-1}, Table S1) to the toluene phase containing OLA is 5:1. Accordingly, the amount of OLA-$Au_{5.5}$@$Ag_{5.25}$ NPs for assembly is 1.9×10^{13}, which was stored in the toluene phase in our case.

$$V = \frac{N}{C_{\mathrm{NUM}}} \qquad (2)$$

The volume (V) of the toluene phase is calculated to be about 3.9 mL according to the formula (2), assumed that all of the NPs are completely transfer from the aqueous solution to the toluene phase during the phase transfer without any loss.

In brief, the volume of the toluene phase containing the NPs used for self-assembly can be adjusted according to the real interfacial area, the particle radius and its concentration of particle number. Accordingly, the volume of the toluene phase containing OLA-$Au_{5.5}$ NPs, OLA-Au_{16} NPs, OLA-$Au_{5.5}$@$Ag_{1.25}$ NPs and OLA-$Au_{5.5}$@$Ag_{3.25}$ NPs in our case are calculated to be 1.1, 3.2, 15.6, and 6.9 mL, respectively.

For comparison, large-area films with disordered arrays of $Au_{5.5}$@$Ag_{5.25}$ NPs (LAF-DOA-$Au_{5.5}$@$Ag_{5.25}$ NPs, **Figure S7**) were prepared by dropping the toluene solution (25 μL) containing OLA-$Au_{5.5}$@$Ag_{5.25}$ NPs onto the substrate in an area of 0.5×0.5 cm^2 and drying in air. The amount (25 μL) of the NPs used is also calculated by the same method above, assume that all of the NPs are closely packed in a monolayer on the surface of the PDMS substrate within an area of 0.5×0.5 cm^2.

Stability Test of LAMF-HCP-Au@Ag NPs. The stability of the LAMF-HCP-Au@Ag NPs (say, soaking in acid or alkali media, and long-term storage in air and under sunlight) was investigated. In detail, the as-prepared LAMF-HCP-Au@Ag NP@PDMS were soaked in the

aqueous solutions (pH=1 and 13) for 1 h and then dried with N2 gas for SERS measurements. The pH values of the aqueous solutions were adjusted with HCl solution or NaOH solution, respectively, and then were determined by one pH-meter. And the volumes of all the aqueous solutions were fixed as 2 mL. For long-term durability, the as-prepared LAMF-HCP-Au@Ag NP@PDMS were stored for different days (0, 5, 10 and 15 days) in air and under sunlight for SERS measurements.

SERS Measurements. Crystal violet (CV) and 4-aminothiophenol (4-ATP) were selected as Raman probes. The as-prepared LAMF-HCP-Au@Ag NPs were transferred onto PDMS (LAMF-HCP-Au@Ag NP@PDMS) as SERS substrates. The SERS substrates were immersed in aqueous solutions containing different concentrations of CV (or 4-ATP) probes (ranging from 10^{-14} to10^{-6} M) for 1 hour. The SERS substrates were then thoroughly rinsed with ethanol and dried with N_2 gas for subsequent testing. The volumes of the aqueous solutions of the analytes of various concentrations were fixed to 2 mL. The performance of the as-prepare SERS substrates was further investigated by extending the immersing time (ranging from 1 to 12 h) in aqueous solutions. The other test parameters were the same as those used above. As general parameters of the Raman spectrometer, the wavelength of the Raman laser and the acquisition time are 633 nm and 10 s, respectively. The laser power is generally selected as 0.0425 mW without additional explanations, while the laser power is reduced to 0.0085 mW if the signal intensities of the SERS spectra exceed the measuring range of the spectrometer.

Enhancement Factor Calculations. The calculation of the enhancement factor (EF) based on the following equation (3):[1,2]

$$\mathrm{EF} = \frac{I_{\mathrm{SERS}} N_{\mathrm{normal}}}{I_{\mathrm{normal}} N_{\mathrm{SERS}}} \qquad (3)$$

where I_{SERS} is the intensity of the characteristic peak of the SERS spectra of the probes; I_{normal} is the intensity of the same peak of the normal Raman spectra of the probes under the same conditions (**Table S6**); N_{normal} is the number of probe molecules in the excitation volume for the normal Raman measurements; N_{SERS} is the number of adsorbed molecules on the films in the excitation volume contributing to I_{SERS}.

The N_{normal} is estimated by using the following equations (4) and (5):

$$V = \pi r^2 h \qquad (4)$$

$$N_{normal} = \left(\frac{\rho V}{M}\right) N_{\mathrm{A}} \qquad (5)$$

where r is the radius of the beam size (0.75 μm), h is the effective depth of the beam focus (2 μm), ρ is the density of CV probes (1.19 g/mL), M is the molar mass of CV probes (407.99 g/mol), N_{A} is the Avogadro constant (6.02×10^{23} $\mathrm{mol^{-1}}$).

It is known that the first monolayer gives the largest contribution to SERS spectra, therefore we assumed that the CV molecules were adsorbed as a closely packed monolayer with a molecular footprint of 1.51 $\mathrm{nm^2}$. The surface area of the monolayer film on the beam can be estimated by the corresponding calculation (πr^2, in which r is the radius of the beam size). Based on the surface areas of the monolayer film on the beam and single CV molecule, the N_{SERS} can be estimated.

In our case, the characteristic peak of CV probes at 1617 $\mathrm{cm^{-1}}$ is chosen for the EF calculations. Therefore, their EFs are estimated accordingly (**Table S6**).

Characterizations. The morphology and structure of the products were obtained with a JEOL JEM-2100F transmission electron microscope (TEM) operating with an acceleration voltage of 200 kV. Elemental mapping images were observed by energy dispersive X-ray spectroscopy (EDS) using a JEOL-2100F scanning transmission electron microscope (STEM). The extinction spectra were recorded using a Cary 50 spectrophotometer. All of the SERS spectra were obtained at room temperature using a Renishaw inVia Reflex Raman spectrometer with 633 nm as an excitation wavelength.

Figure S1. TEM image (a) and extinction spectrum (b) of 5.5 nm citrated-stabilized Au NPs in water.

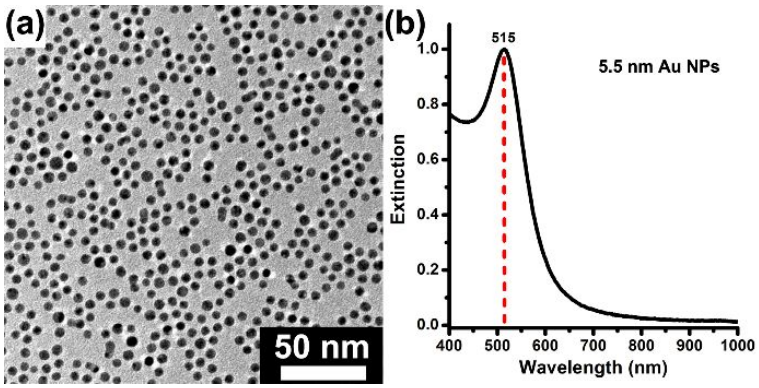

Figure S1a shows the typical TEM image of quasi-spherical, citrate-stabilized Au NPs obtained by the premixing protocol. In general, 2.5 mL of an aqueous solution of sodium citrate (1 wt %) and 0.5 mL of an aqueous solution of $HAuCl_4$ (25 mM) were premixed and stirred for about 12 min at room temperature. After the premixture turns dark green, the premixture was quickly added into 47 mL of the boiling water under vigorous stirring. After continuous heating and stirring for 30 min, the resulting solution with a light red color was obtained, which was naturally cooled to room temperature under stirring. Eventually, a dispersion containing citrate-stabilized Au NPs was obtained. Their average size was determined to be about 5.5 nm according to the statistical analysis from TEM image (**Figure S1a**). In addition, these Au NPs show one surface plasmon resonance (SPR) band with a narrow half-width in water and their center position is near 515 nm, as shown in **Figure S1b**.

Figure S2. TEM images of 8 nm $Au_{5.5}@Ag_{1.25}$ NPs (a), 12 nm $Au_{5.5}@Ag_{3.25}$ NPs (b), 16 nm $Au_{5.5}@Ag_{5.25}$ NPs (c) and their corresponding extinction spectra (d) in water. The extinction spectra in (d) are normalized by the intensity of their SPR peaks.

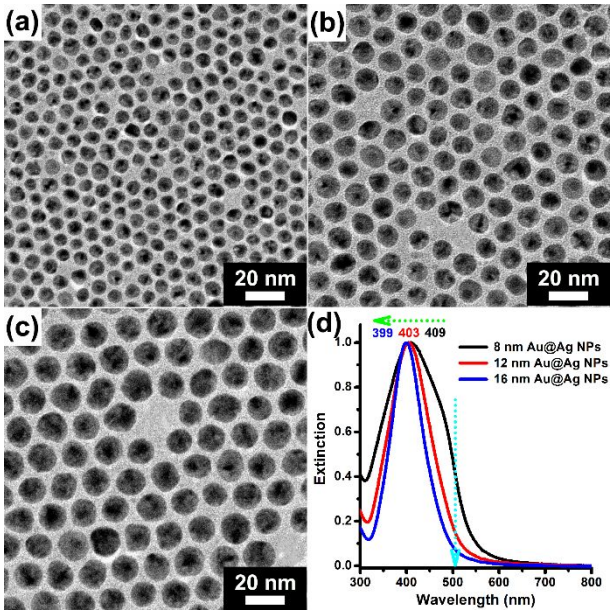

Figure S2a-2c show the typical TEM images of quasi-spherical, citrate-stabilized core-shell structured (CS) $Au_{5.5}@Ag_m$ NPs with Ag shells of different thicknesses (m presents the thickness of Ag shell) obtained by reducing silver-ammonia complex with AA. According to the statistical analysis (**Table S2**) from their TEM images, the total sizes of the resulting $Au_{5.5}@Ag_m$ NPs are determined to be 8 ± 0.7, 12 ± 1, and 16 ± 1.2 nm, respectively. Accordingly, the average thicknesses of Ag shells of the resulting $Au_{5.5}@Ag_m$ NPs are about 1.25, 3.25, and 5.25 nm, respectively, since the average size of Au NP-cores is about 5.5 nm. **Figure S2d** shows their corresponding extinction spectra. Since the presence of the SPR of the Au cores (**Figure S1b**), the SPR peak of $Au_{5.5}@Ag_m$ NPs with thin Ag shells of different thickness are indeed affected. When the thickness of Ag shells on $Au_{5.5}$ NPs is about 1.25 nm,

the center position of the dipolar resonance peak of 8 nm $Au_{5.5}@Ag_{1.25}$ NPs blueshifts from 515 to 409 nm. In addition, the dipolar resonance peak of Au cores (about 515 nm) has almost disappeared while a shoulder peak around 470 nm appears. When the thickness of Ag shells increases to 3.25 nm, the center position of the dipolar resonance peak of 12 nm $Au_{5.5}@Ag_{3.25}$ NPs blueshifts from 515 to 403 nm. In addition, the dipolar resonance peak of Au cores (about 515 nm) has completely disappeared while the shoulder peak also disappears. When the thickness of Ag shells further increases to 5.25 nm, the center position of the dipolar resonance peak of 16 nm $Au_{5.5}@Ag_{5.25}$ NPs blueshifts from 515 to 399 nm. In addition, the dipolar SPR peak is rather similar to that of pure Ag NPs of comparable size and is also relatively symmetrical with a narrow half-width.

Figure S3. HAADF-STEM image (a), HAADF-STEM-EDS mapping images (b and c), and their overlapped image (d) of 8 nm $Au_{5.5}@Ag_{1.25}$ NPs. The inset in (a) is the cross-sectional compositional line profile of a single $Au_{5.5}@Ag_{1.25}$ NP.

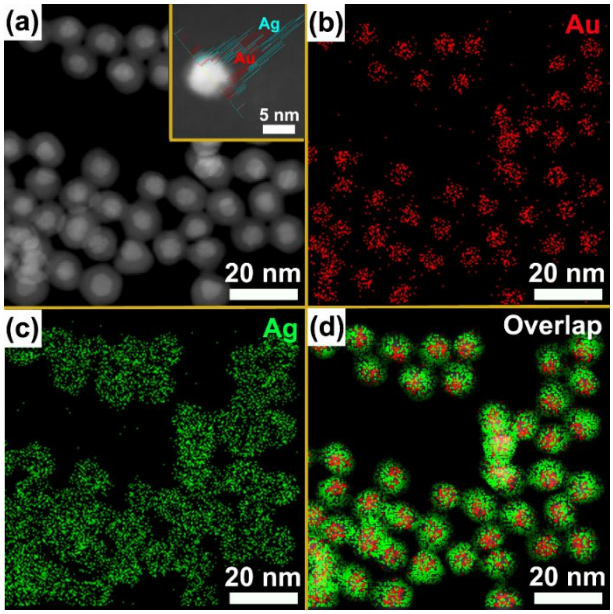

As shown in their HAADF-STEM image (**Figure S3a**), the as-prepared 8 nm $Au_{5.5}@Ag_{1.25}$ NPs are composed of bright cores and dark shells, which are also demonstrated by the result of the cross-sectional compositional line profile of one individual $Au_{5.5}@Ag_{1.25}$ NP (inset in **Figure S3a**). Moreover, elemental Au and elemental Ag in their HAADF-STEM-EDS mapping images (**Figure S3b and Figure S3c**) display small and big quasi-spherical shapes, respectively. Furthermore, in their overlapped image (**Figure S3d**), elemental Au are completely enclosed by elemental Ag, indicating that the 8 nm $Au_{5.5}@Ag_{1.25}$ NPs have a core-shell structure. All of results (**Figure S3**) demonstrate the formation of core-shell structure in the as-prepared 8 nm $Au_{5.5}@Ag_{1.25}$ NPs.

Figure S4. HAADF-STEM image (a), HAADF-STEM-EDS mapping images (b and c), and their overlapped image (d) of 12 nm $Au_{5.5}@Ag_{3.25}$ NPs. The inset in (a) is the cross-sectional compositional line profile of a single $Au_{5.5}@Ag_{3.25}$ NP.

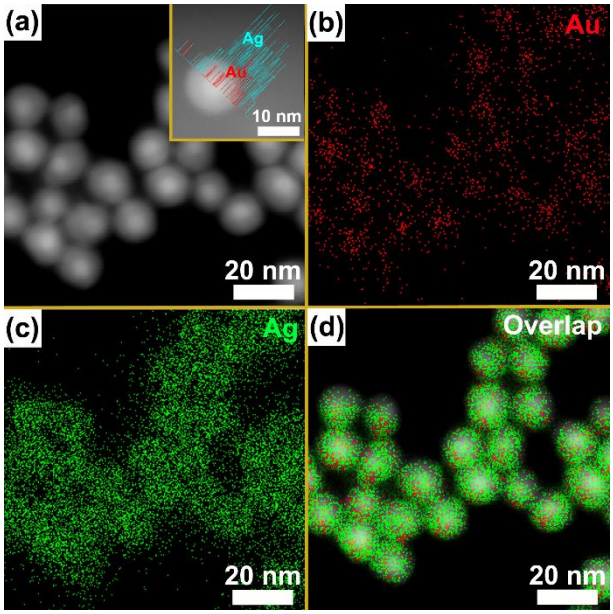

Similar to the characterizations of 8 nm $Au_{5.5}@Ag_{1.25}$ NPs (**Figure S3**), all of results (**Figure S4**) demonstrate the formation of core-shell structure in the as-prepared 12 nm $Au_{5.5}@Ag_{3.25}$ NPs.

Figure S5. Optical photo (a) of LAMF-HCP-$Au_{5.5}$@$Ag_{1.25}$ NPs on the DEG surface and their low (b, c) and high (d, e) magnification TEM images, the extinction spectrum (f) of LAMF-HCP-$Au_{5.5}$@$Ag_{1.25}$ NP@PDMS substrate. Insets in (c) and (f) are the corresponding FFT pattern and the optical photo, respectively.

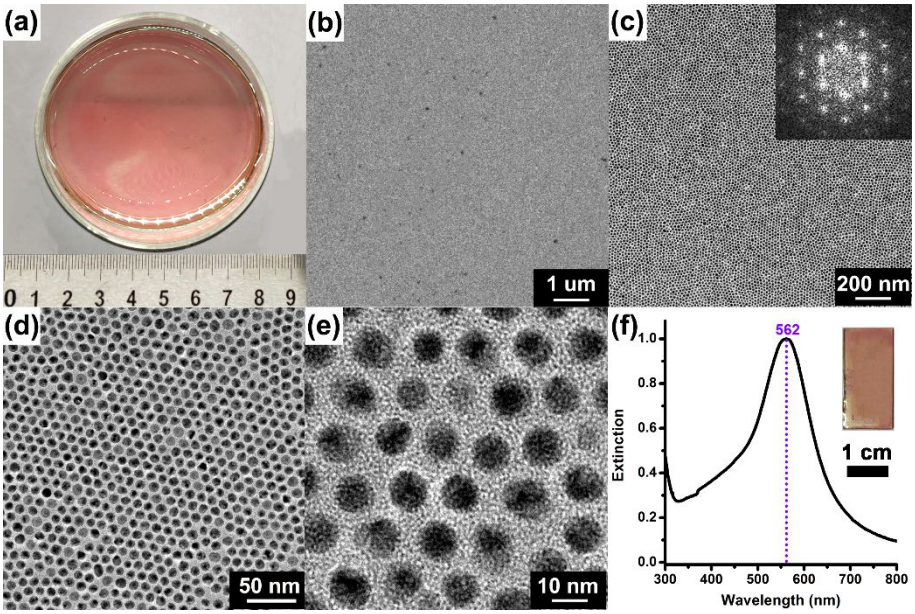

As shown in **Figure S5a**, the resulting LAMF-HCP-$Au_{5.5}$@$Ag_{1.25}$ NPs on the surface of DEG phase shows a light pink color and their area can be up to 30 cm^2. As shown in the low magnification TEM image (**Figure S5b**), there are hardly big voids, cracks and agglomerates observed in the area of about 64 μm^2, indicating the high quality of the as-prepared LAMF. And $Au_{5.5}$@$Ag_{1.25}$ NPs in the LAMF are in an ordered arrangement (**Figure S5c**), which is evidenced by the fast Fourier transform (FFT) pattern (inset in **Figure S5c**) with a clear hexagonal point-like array performed by the selected area in the TEM image. Moreover, the hexagonal close-packed (HCP) arrangement of $Au_{5.5}$@$Ag_{1.25}$ NPs in the LAMF is further revealed by their HRTEM images (**Figure S5d and S5e**). And the average spacing among NPs

is about 2.0 ± 0.5 nm. The center position of the SPR peak with a narrow half-width of the LAMF-HCP-$Au_{5.5}$@$Ag_{1.25}$ NP@PDMS is near 562 nm (**Figure S5f**).

Figure S6. Optical photo (a) of LAMF-HCP-$Au_{5.5}$@$Ag_{3.25}$ NPs on the DEG surface and their low (b, c) and high (d, e) magnification TEM images, the extinction spectrum (f) of LAMF-HCP-$Au_{5.5}$@$Ag_{3.25}$ NP@PDMS substrate. Insets in (c) and (f) are the corresponding FFT pattern and the optical photo, respectively.

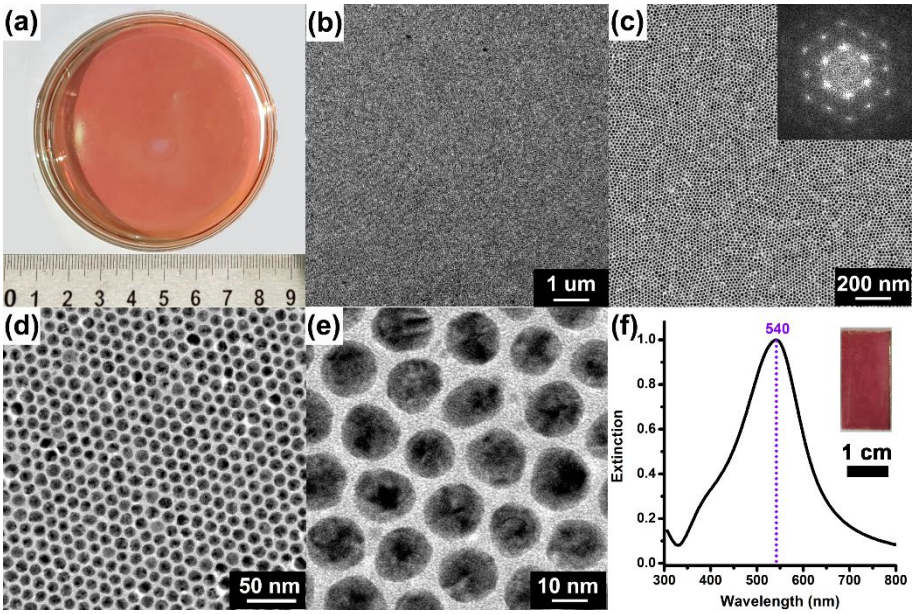

As shown in **Figure S6a**, the resulting LAMF-HCP-$Au_{5.5}$@$Ag_{3.25}$ NPs on the surface of DEG phase shows a tangerine color and their area can be up to 30 cm^2. As shown in the low magnification TEM image (**Figure S6b**), there are hardly big voids, cracks and agglomerates observed in the area of about 64 μm^2, indicating the high quality of the as-prepared LAMF. And $Au_{5.5}$@$Ag_{3.25}$ NPs in the LAMF are in an ordered arrangement (**Figure S6c**), which is evidenced by the FFT pattern (inset in **Figure S6c**) with a clear hexagonal point-like array performed by the selected area in the TEM image. Moreover, the HCP arrangement of $Au_{5.5}$@$Ag_{3.25}$ NPs in the LAMF is further revealed by their HRTEM images (**Figure S6d and S6e**). And the average spacing among NPs is about 1.9 ± 0.5 nm. The center position of the

SPR peak with a narrow half-width of the LAMF-HCP-$Au_{5.5}$@$Ag_{3.25}$ NP@PDMS is near 540 nm (**Figure S6f**).

Figure S7. (a) Low magnification TEM image of LAFs with disordered arrays of $Au_{5.5}@Ag_{5.25}$ NPs (LAF-DOA-$Au_{5.5}@Ag_{5.25}$ NPs) on copper grids. (b) Extinction spectrum of DOA-$Au_{5.5}@Ag_{5.25}$ NPs transferred on PDMS (DOA-$Au_{5.5}@Ag_{5.25}$ NP@PDMS). The inset in (b) is the optical photo of the resulting DOA-$Au_{5.5}@Ag_{5.25}$ NP@PDMS.

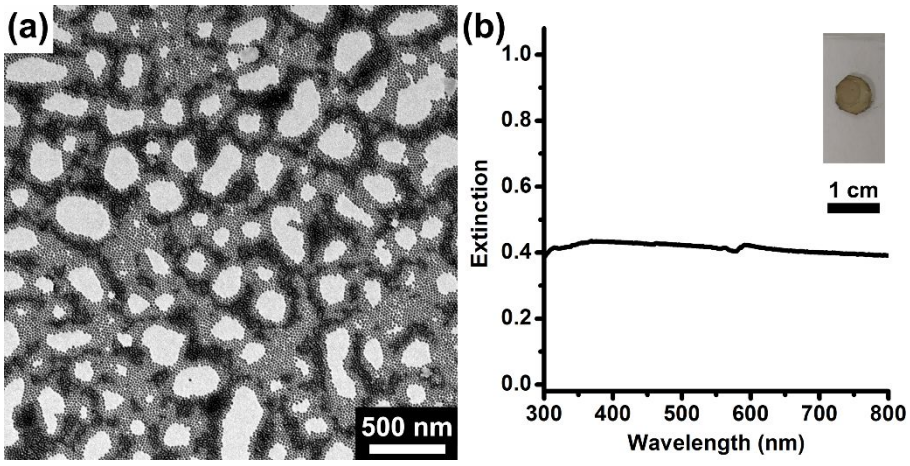

Figure S8. (a) SERS spectra of CV probes (10^{-6} M) adsorbed on DOA-$Au_{5.5}$@$Ag_{5.25}$ NP@PDMS. (b) Color-map of the signal intensity of the peak at 1617 cm^{-1} obtained from the corresponding SERS spectra. (c) Histogram of the intensity of the peak at 1617 cm^{-1} in the corresponding SERS spectra. The power of the laser is 0.0085 mW.

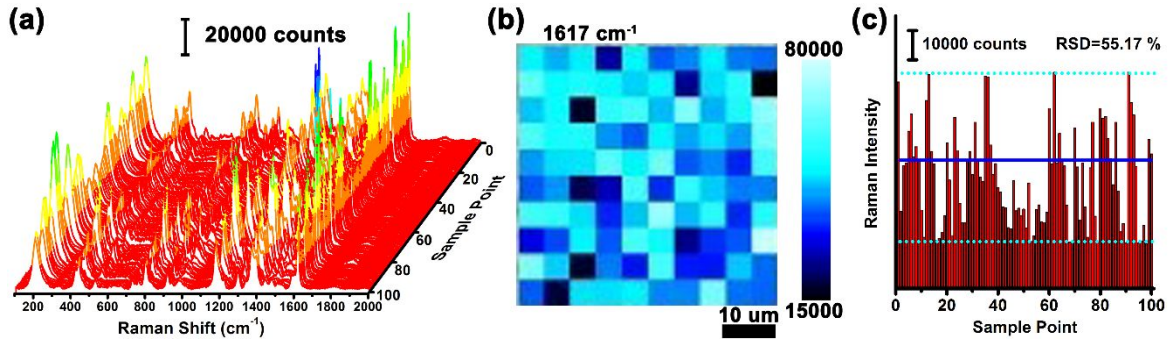

Figure S8a shows the SERS spectra of CV probes (10^{-6} M) adsorbed on DOA-$Au_{5.5}$@$Ag_{5.25}$ NP@PDMS obtained at 100 different positions in a square area of 50 × 50 μm^2 with regular distance of 5 μm. It can be clearly seen that the uniformity and reproducibility in their SERS signals are rater lower by using the DOA-$Au_{5.5}$@$Ag_{5.25}$ NP@PDMS as SERS substrates (**Figure S8b**), compared with those of LAMF-HCP-$Au_{5.5}$@$Ag_{5.25}$ NP@PDMS (**Figure 4b**). As expected, the RSD in the intensity of the CV characteristic peaks at about 1617 cm^{-1} in SERS spectra is up to 55.17 % (**Figure S8c**), which is much bigger than that of LAMF-HCP-$Au_{5.5}$@$Ag_{5.25}$ NP@PDMS (**Figure 4c**).

Figure S9. (a) SERS spectra of CV probes (10^{-6} M) adsorbed on LAMF-HCP-$Au_{5.5}$@$Ag_{1.25}$ NP@PDMS. (b) Color-map of the signal intensity of the peak at 1617 cm^{-1} obtained from the corresponding SERS spectra. (c) Histogram of the intensity of the peak at 1617 cm^{-1} in the corresponding SERS spectra. The power of the laser is 0.0085 mW.

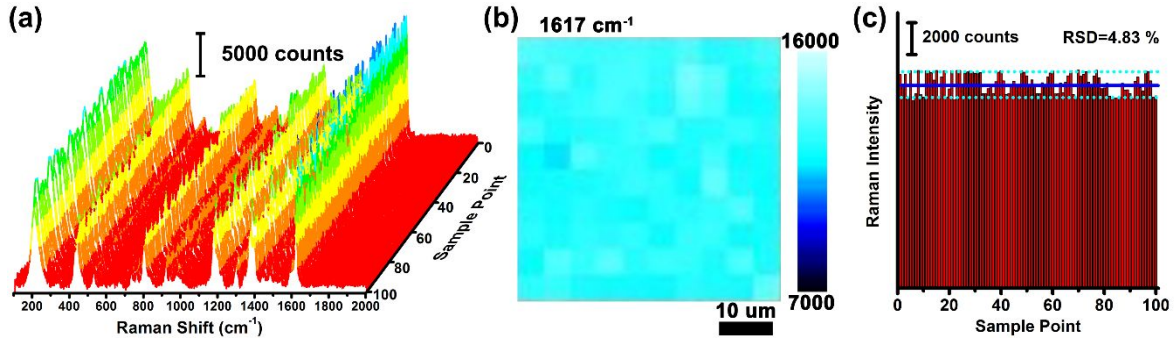

Figure S9a shows the SERS spectra of CV probes (10^{-6} M) adsorbed on LAMF-HCP-$Au_{5.5}$@$Ag_{1.25}$ NP@PDMS obtained at 100 different positions in a square area of 50 μm × 50 μm with regular distance of 5 μm. It can be clearly seen that the uniformity and reproducibility in their SERS signals are rather close to those of LAMF-HCP-$Au_{5.5}$@$Ag_{5.25}$ NP@PDMS (**Figure 4b**) by using the as-prepared LAMF-HCP-$Au_{5.5}$@$Ag_{1.25}$ NP@PDMS as SERS substrates (**Figure S9b**). As expected, the RSD in the intensity of the CV characteristic peaks at about 1617 cm^{-1} in SERS spectra is 4.83 % (**Figure S9c**), which is also much close to that of LAMF-HCP-$Au_{5.5}$@$Ag_{5.25}$ NP@PDMS (**Figure 4c**).

Figure S10. (a) SERS spectra of CV probes (10^{-6} M) adsorbed on LAMF-HCP-$Au_{5.5}$@$Ag_{3.25}$ NP@PDMS. (b)Color-map of the signal intensity of the peak at 1617 cm^{-1} obtained from the corresponding SERS spectra. (c) Histogram of the intensity of the peak at 1617 cm^{-1} in SERS spectra. The power of the laser is 0.0085 mW.

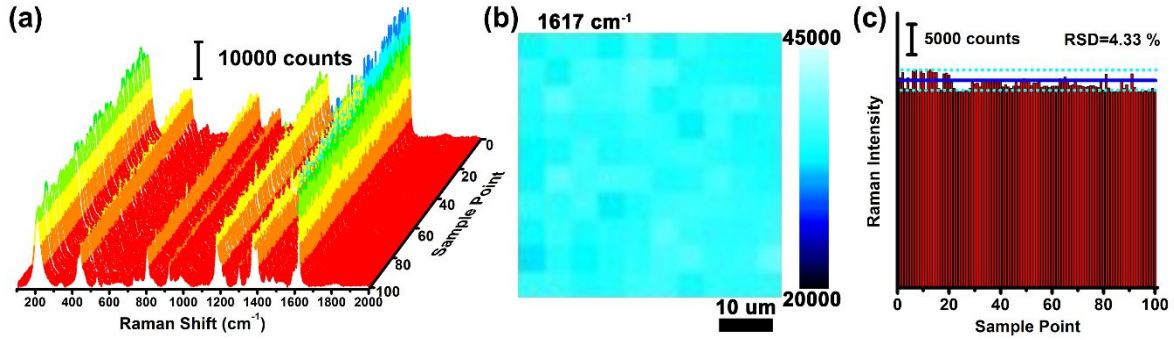

Figure S10a shows the SERS spectra of CV probes (10^{-6} M) adsorbed on LAMF-HCP-$Au_{5.5}$@$Ag_{3.25}$ NP@PDMS obtained at 100 different positions in a square area of 50 μm × 50 μm with regular distance of 5 μm. It can be clearly seen that the uniformity and reproducibility in their SERS signals are rather close to those of LAMF-HCP-$Au_{5.5}$@$Ag_{5.25}$ NP@PDMS (**Figure 4b**) by using the as-prepared LAMF-HCP-$Au_{5.5}$@$Ag_{3.25}$ NP@PDMS as SERS substrates (**Figure S10b**). As expected, the RSD in the intensity of the CV characteristic peaks at about 1617 cm^{-1} in SERS spectra is 4.33 % (**Figure S10c**), which is also much close to that of LAMF-HCP-$Au_{5.5}$@$Ag_{5.25}$ NP@PDMS (**Figure 4c**)

Figure S11. Optical photo (a) of LAMF-HCP-Au_{16} NPs on the DEG surface and their low (b, c) and high (d, e) magnification TEM images, the extinction spectrum (f) of LAMF-HCP-Au_{16} NP@PDMS substrate. Insets in (c) and (f) are the corresponding FFT pattern and the optical photo, respectively.

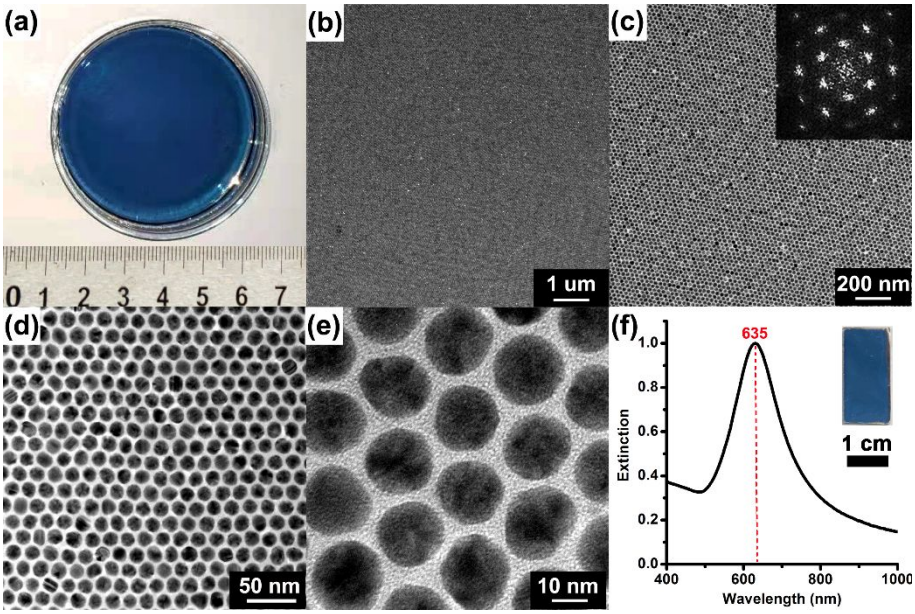

As shown in **Figure S11a**, the resulting LAMF-HCP-Au_{16} NPs on the surface of DEG phase shows a deep blue color and their area can be up to 30 cm^2. As shown in the low magnification TEM image (**Figure S11b**), there are hardly big voids, cracks and agglomerates observed in the area of about 64 μm^2, indicating the high quality of the as-prepared LAMF. And Au_{16} NPs in the LAMF are in an ordered arrangement (**Figure S11c**), which is evidenced by the FFT pattern (inset in **Figure S11c**) with a clear hexagonal point-like array performed by the selected area in the TEM image. Moreover, the HCP arrangement of Au_{16} NPs in the LAMF is further revealed by their HRTEM images (**Figure S11d and S11e**). And the average spacing among NPs is about

1.7 ± 0.6 nm. The center position of the SPR peak with a narrow half-width of the LAMF-HCP-Au_{16} NP@PDMS is near 635 nm (**Figure S11f**).

Figure S12. (a) SERS spectra of CV probes (10^{-6} M) adsorbed on LAMF-HCP-Au_{16} NP@PDMS. (b) Color-map of the signal intensity of the peak at 1617 cm^{-1} obtained from the corresponding SERS spectra. (c) Histogram of the intensity of the peak at 1617 cm^{-1} in the corresponding SERS spectra. The power of the laser is 0.0085 mW.

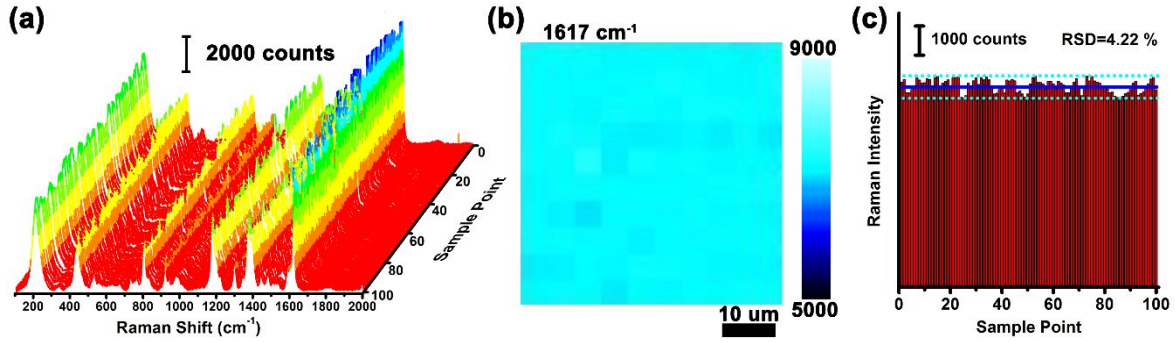

Figure S12a shows the SERS spectra of CV probes (10^{-6} M) adsorbed on LAMF-HCP-Au_{16} NP@PDMS obtained at 100 different positions in a square area of 50 × 50 μm^2 with regular distance of 5 μm. It can be clearly seen that the uniformity and reproducibility in their SERS signals are also rather close to those of LAMF-HCP-$Au_{5.5}$@$Ag_{5.25}$ NP@PDMS (**Figure 4b**) by using the as-prepared LAMF-HCP-Au_{16} NP@PDMS as SERS substrates (**Figure S12b**). As expected, the RSD in the intensity of the CV characteristic peaks at about 1617 cm^{-1} in SERS spectra is 4.22 % (**Figure S12c**), which is also much close to that of LAMF-HCP-$Au_{5.5}$@$Ag_{5.25}$ NP@PDMS (**Figure 4c**).

Figure S13. Optical photo (a) of LAMF-HCP-$Au_{5.5}$ NPs on the DEG surface and their low (b, c) and high (d, e) magnification TEM images, the extinction spectrum (f) of LAMF-HCP-$Au_{5.5}$ NP@PDMS substrate. Insets in (c) and (f) are the corresponding FFT pattern and the optical photo, respectively.

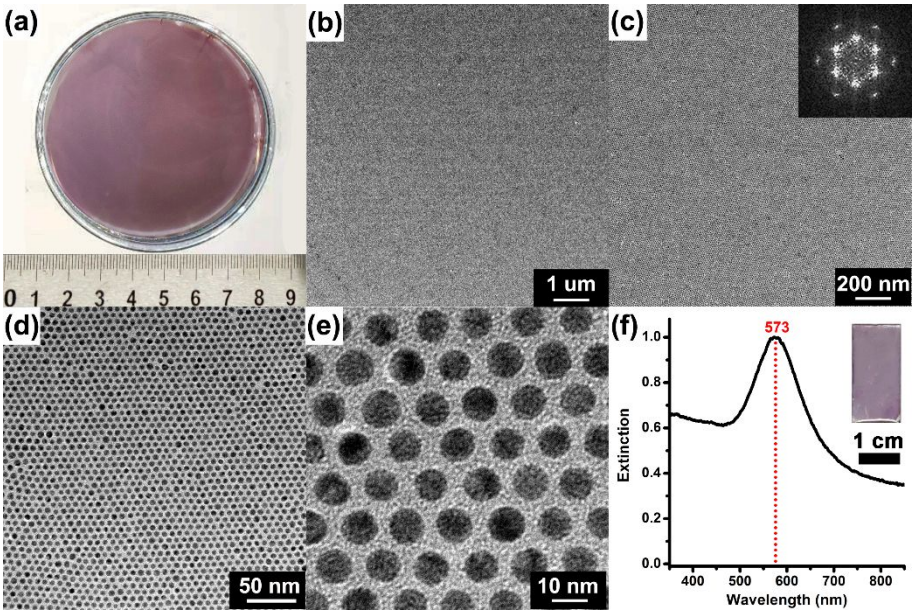

As shown in **Figure S13a**, the resulting LAMF-HCP-$Au_{5.5}$ NPs on the surface of DEG phase shows a light purple color and their area can be up to 30 cm^2. As shown in the low magnification TEM image (**Figure S13b**), there are hardly big voids, cracks and agglomerates observed in the area of about 64 μm^2, indicating the high quality of the as-prepared LAMF. And $Au_{5.5}$ NPs in the LAMF are in an ordered arrangement (**Figure S13c**), which is evidenced by the FFT pattern (inset in **Figure S13c**) with a clear hexagonal point-like array performed by the selected area in the TEM image. Moreover, the HCP arrangement of $Au_{5.5}$ NPs in the LAMF is further revealed by their HRTEM images (**Figure S13d and S13e**). And the average spacing among NPs is about

2.0 ± 0.6 nm. The center position of the SPR peak with a narrow half-width of the LAMF-HCP-$Au_{5.5}$ NP@PDMS is near 573 nm (**Figure S13f**).

Figure S14. (a) SERS spectra of CV probes (10^{-6} M) adsorbed on LAMF-HCP-$Au_{5.5}$ NP@PDMS. (b) Color-map of the signal intensity of the peak at 1617 cm^{-1} obtained from the corresponding SERS spectra. (c) Histogram of the intensity of the peak at 1617 cm^{-1} in the corresponding SERS spectra. The power of the laser is 0.0085 mW.

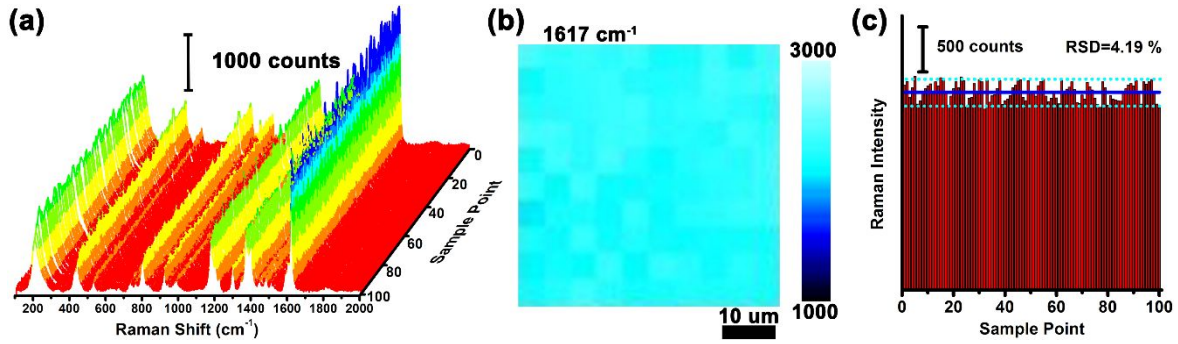

Figure S14a shows the SERS spectra of CV probes (10^{-6} M) adsorbed on LAMF-HCP-$Au_{5.5}$ NP@PDMS obtained at 100 different positions in a square area of 50 × 50 μm^2 with regular distance of 5 μm. It can be clearly seen that the uniformity and reproducibility in their SERS signals are also rather close to those of LAMF-HCP-$Au_{5.5}$@$Ag_{5.25}$ NP@PDMS (**Figure 4b**) by using the as-prepared LAMF-HCP-$Au_{5.5}$ NP@PDMS as SERS substrates (**Figure S14b**). As expected, the RSD in the intensity of the CV characteristic peaks at about 1617 cm^{-1} in SERS spectra is 4.19 % (**Figure S14c**), which is also much close to that of LAMF-HCP-$Au_{5.5}$@$Ag_{5.25}$ NP@PDMS (**Figure 4c**).

Figure S15. (a) Typical SERS spectra of CV probes (10^{-6} M) adsorbed on LAMF-HCP-$Au_{5.5}$@$Ag_{5.25}$ NP@PDMS before and after acid (pH=1) and alkali (pH=13) treatments. (b) Typical SERS spectra of CV probes (10^{-6} M) adsorbed on LAMF-HCP-$Au_{5.5}$@$Ag_{5.25}$ NP@PDMS before and after the long-term storage (5, 10 and 15 days) in air and under sunlight. The power of the laser is 0.0085 mW.

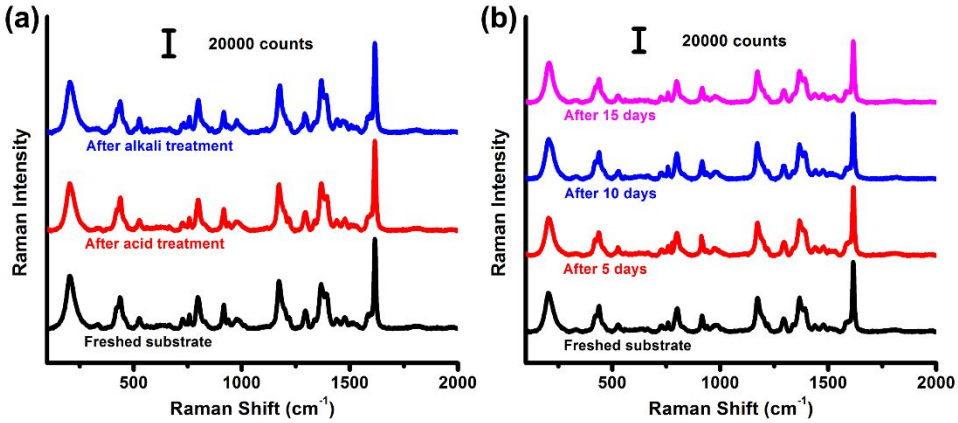

The SERS spectra of CV probes adsorbed on LAMF-HCP-$Au_{5.5}$@$Ag_{5.25}$ NP@PDMS before and after the treatments (soaking them into the acidic (pH=1) and alkali media (pH=13) for 1 h) are almost the same (**Figure S15a**). These results indicate that the as-prepared LAMF-HCP-Au@Ag NP@PDMS is rather stable in acidic and alkali media as the SERS-based detector.

In addition, the SERS spectra (**Figure S15b**) of CV probes adsorbed on LAMF-HCP-$Au_{5.5}$@$Ag_{5.25}$ NP@PDMS before and after the long-term storage (5, 10 and 15 days) in air and under sunlight are almost the same. These results indicate that the as-prepared LAMF-HCP-Au@Ag NP@PDMS is rather stable when they are exposed in air and under sunlight as the SERS-based detector.

Figure S16. TEM images of LAMF-HCP-$Au_{5.5}$@$Ag_{5.25}$ NPs after soaking in the acidic solution (a, pH=1, HCl) for 1 h and the alkali solution (b, pH=13, NaOH) for 1 h.

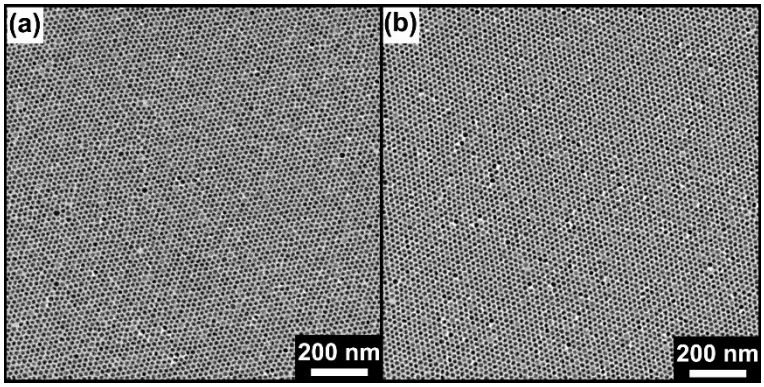

Figure S17. Typical SERS spectra of different concentrations (from 10^{-13} to 10^{-7} M) of CV probes adsorbed on LAMF-HCP-$Au_{5.5}$@$Ag_{5.25}$ NP@PDMS for 1 h.

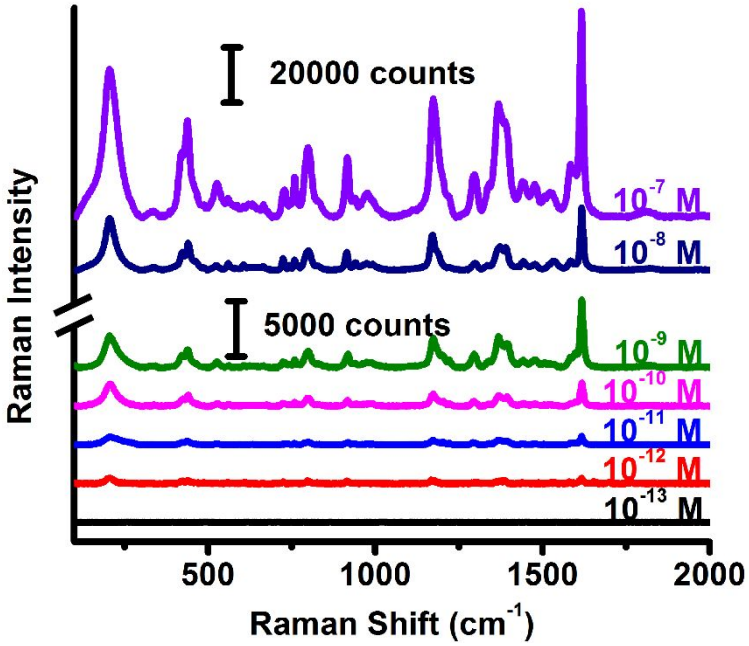

Since the main characteristic peaks can still be observed at the concentration of 10^{-12} M and the signal-to-noise ratio (S/N) is greater than 3 (**Figure S17**), the limit of detection (LOD) of LAMF-HCP-$Au_{5.5}$@$Ag_{5.25}$ NP@PDMS for CV probes is determined to be 10^{-12} M.

Figure S18. SERS spectrum of CV probes (3×10^{-9} M) adsorbed on LAMF-HCP-$Au_{5.5}$@$Ag_{5.25}$ NP@PDMS for 1 h.

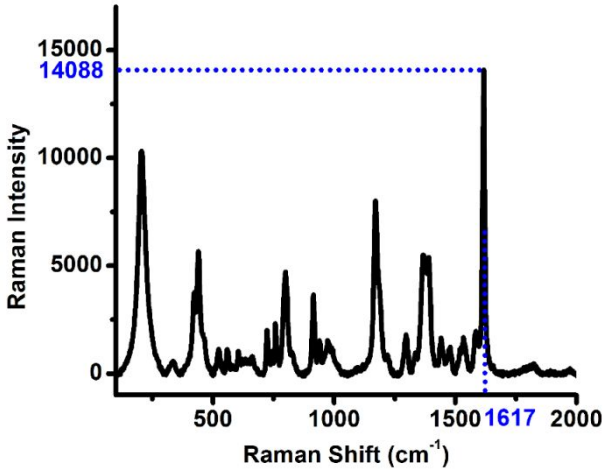

On the basis of the intensity (14088) at 1617 cm^{-1} in the SERS spectrum of the standard sample (**Figure S18**) and the established standard work curve (**Figure 7a**), the CV concentration of the standard sample is calculated to be 2.92×10^{-9} M, which is almost equal to the actual one.

Figure S19. Typical SERS spectra of different concentrations (from 10^{-14} to 10^{-7} M) of 4-ATP probes adsorbed on LAMF-HCP-$Au_{5.5}$@$Ag_{5.25}$ NP@PDMS for 1 h.

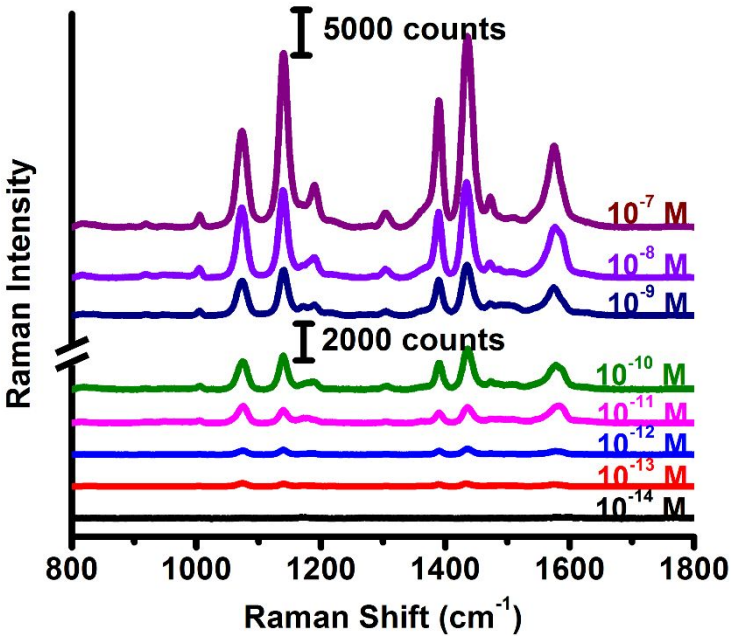

Since the main characteristic peaks can still be observed at the concentration of 10^{-13} M and the signal-to-noise ratio (S/N) is greater than 3 (**Figure S19**), the LOD of LAMF-HCP-$Au_{5.5}$@$Ag_{5.25}$ NP@PDMS for 4-ATP probes is determined to be 10^{-13} M.

Figure S20. SERS spectrum of 4-ATP probes (3×10^{-9} M) adsorbed on LAMF-HCP-$Au_{5.5}$@$Ag_{5.25}$ NP@PDMS for 1 h.

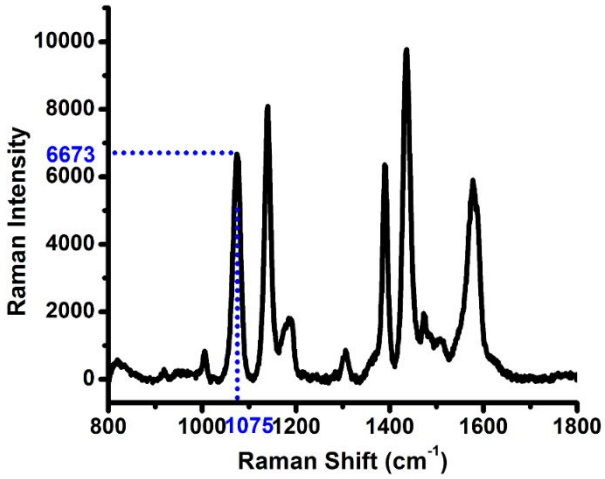

On the basis of the intensity (6673) at 1075 cm^{-1} in the SERS spectrum of the standard sample (**Figure S20**) and the established standard work curve (**Figure 7b**), the concentration of 4-ATP is calculated to be 3.05×10^{-9} M, which is almost equal to the actual one.

Table S1. Summarized recipes of the preparation of $Au_{5.5}@Ag_m$ NPs with Ag shells of different thicknesses by using 5.5 nm Au NPs as cores (m represents the thickness of Ag shells).

Particle size [nm]	8	12	16
Thickness of Ag shells [nm] [a)]	1.25	3.25	5.25
N_{sum} [$*10^{12}$] [b)]	5.86	5.86	5.86
Concentration of $AgNO_3$ [μM]	17	78	195
Concentration of ammonia water [mM] [c)]	45	45	45
Concentration of AA [μM]	35	160	400
Total volume [mL] [d)]	6	6	6

[a] The average thickness of Ag shells of $Au_{5.5}@Ag_m$ NPs are calculated by subtracting the average size of Au-NP cores (5.5 nm) from the total sizes of the resulting $Au_{5.5}@Ag_m$ NPs obtained from their statistical analysis from their TEM images (**Table S2**); [b] the particle number of 5.5 nm Au-NP cores added into the reaction solution by calculation, which is equal to the particle number of $Au_{5.5}@Ag_m$ NPs; [c] the concentration of ammonia water used for mixing with the aqueous solution of $AgNO_3$ to prepare the aqueous solution of silver-ammonia complex; [d] the total volume of the reaction solutions is fixed to 6 mL.

Table S2. Summarized data of TEM images of the resulting $Au_{5.5}@Ag_m$ NPs in **Figure S2**.

Sample image	Measured size [nm]	Ellipticity [a)]	Deviation [%] [b)]
Figure S2a	8 ± 0.7	1.09	8.75
Figure S2b	12 ± 1	1.08	8.33
Figure S2c	16 ± 1.2	1.06	7.50

[a] The ellipticity of the morphology is estimated as the ratio of the major to minor axes; [b] the standard deviation of the size is estimated as the distribution of the large to small diameters.

Table S3. Summarized data of the signal intensities of CV characteristic peaks in the SERS spectra measured on the substrates based on different NPs with comparable size (**Figure 5a**).

	Raman shift [cm^{-1}]	207	441	1170	1387	1617
Raman intensity	LAMF-HCP-Au_{16} NP@PDMS	5183	2762	4121	3273	8611
	LAMF-HCP-$Au_{5.5}$@$Ag_{5.25}$ NP@PDMS	51465	31648	47638	32989	77391

Table S4. Summarized data of the signal intensities of 4-ATP characteristic peaks in the SERS spectra measured on the substrates based on different NPs with comparable size (**Figure 5b**).

	Raman shift [cm^{-1}]	1075	1140	1390	1435	1580
Raman intensity	LAMF-HCP-Au_{16} NP@PDMS	4074	1812	1579	2028	3237
	LAMF-HCP-$Au_{5.5}$@$Ag_{5.25}$ NP@PDMS	58941	90271	68472	103731	47662

Table S5. Summarized data of the signal intensities of CV characteristic peaks in the SERS spectra measured on different substrates with ordered arrays (**Figure 6b**).

	Raman shift [cm^{-1}]	207	441	1170	1387	1617
Raman intensity	LAMF-HCP-$Au_{5.5}$ NP@PDMS	1663	966	1448	1075	2033
	LAMF-HCP-$Au_{5.5}$@$Ag_{1.25}$ NP@PDMS	10188	5439	6181	4773	11375
	LAMF-HCP-$Au_{5.5}$@$Ag_{3.25}$ NP@PDMS	15603	11475	14375	11483	27955
	LAMF-HCP-$Au_{5.5}$@$Ag_{5.25}$ NP@PDMS	51465	31648	47638	32989	77391

Table S6. Summarized data of calculated EFs of various SERS substrates with ordered arrays based on the intensity of the characteristic peak of CV spectra at 1617 cm^{-1} (**Figure 5a and 6b**). The power of the laser is 0.0085 mW.

SERS substrate	Raman intensity (1617 cm^{-1})	EFs [10^6]
None	91*	None
LAMF-HCP-Au_{16} NP@PDMS	8611	5.02
LAMF-HCP-$Au_{5.5}$ NP@PDMS	2033	1.18
LAMF-HCP-$Au_{5.5}$@$Ag_{1.25}$ NP@PDMS	11375	6.63
LAMF-HCP-$Au_{5.5}$@$Ag_{3.25}$ NP@PDMS	27955	16.3
LAMF-HCP-$Au_{5.5}$@$Ag_{5.25}$ NP@PDMS	77391	45.1

* The Raman spectra of CV probes without any substrates cannot be directly obtained at the same conditions (633 nm, 0.0085 mW, 10 s) that were used for the SERS measurement. Thus, their intensity is obtained by tenfold accumulation of the intensity obtained at this condition.

Table S7. Summarized detection data of actual concentrations of CV/4-ATP and calculated concentrations based on the standard fitting curves (**Figure 7**).

Probe	Actual concentration [M]	Raman intensity		Calculated concentration [M]	Standard deviation [%]*
CV	6×10^{-8}	1617 cm^{-1}	64923	6.37×10^{-8}	6.17
	3×10^{-8}		45659	3.13×10^{-8}	4.33
	6×10^{-9}		20322	6.11×10^{-9}	1.83
	6×10^{-10}		6333	5.81×10^{-10}	3.17
	6×10^{-11}		1975	5.53×10^{-11}	7.83
4-ATP	6×10^{-8}	1075 cm^{-1}	19038	5.66×10^{-8}	5.67
	3×10^{-8}		15666	3.29×10^{-8}	9.67
	6×10^{-9}		8590	6.17×10^{-9}	2.83
	6×10^{-10}		3645	5.67×10^{-10}	5.50
	6×10^{-11}		1582	5.55×10^{-11}	7.50

* The standard deviation is calculated from the ratio of the concentration error to the actual concentration.

Table S8. Summarized data of the SERS performance for quantitative detection of various substrates in ordered arrays.

Building block	Size of building block [nm]	Gap [nm]	Raman probe	Range of quantitative detection [M]	LOD [M]	Excitation Wavelength [nm]	References
Ag micro-island	4000	\	CV	10^{-9}-10^{-6}	10^{-9}	532	[3]
Au@Ag flower-shaped NP	500	<10	Thiram	10^{-11}-10^{-7}	10^{-11}	785	[4]
Au@Ag NP	43	3	CV	10^{-9}-10^{-6}	10^{-9}	633	[5]
Au NP	80	\	CV	10^{-11}-10^{-8}	10^{-12}	785	[6]
Au NP	45	2-3	MG	10^{-10}-10^{-6}	10^{-10}	633	[7]
Ag@Cu cicada wing	150	\	CV 4-ATP	10^{-10}-10^{-6} 10^{-11}-10^{-6}	10^{-10} 10^{-11}	532	[8]
Au NP	16	1.6	CV	10^{-10}-10^{-6}	10^{-10}	633	[9]
Au@Ag NP	16	1.8	CV 4-ATP	10^{-12}-10^{-7} 10^{-13}-10^{-7}	10^{-13} 10^{-13}	633	This work

Reference

(1) Zhang, Q.; Large, N.; Wang, H. Gold Nanoparticles with Tipped Surface Structures as Substrates for Single-Particle Surface-Enhanced Raman Spectroscopy: Concave Nanocubes, Nanotrisoctahedra, and Nanostars. *ACS Appl. Mater. Interfaces* **2014**, *6*, 17255–17267.

(2) Wu, C.; He, H.; Song, Y.; Bi, C.; Xing L.; Du, W.; Li, S.; Xia, H. Synthesis of Large Gold Nanoparticles with Deformation Twinnings by One-step Seeded Growth with Cu(II)-Mediated Ostwald Ripening for Determining Nitrile and Isonitrile Groups. *Nanoscale* **2020**, *12*, 16934–16943.

(3) Shi, G.; Wang, M.; Zhu, Y.; Wang, Y.; Xu, H. A Novel Natural SERS System for Crystal Violet Detection Based on Graphene Oxide Wrapped Ag Micro-Islands Substrate Fabricated from Lotus Leaf as a Template. *Appl. Surf. Sci.* **2018**, *459*, 802–811.

(4) Xing, C.; Zhong, S.; Yu, J.; Li, X.; Cao, A.; Men, D.; Wu, B.; Cai, W.; Li, Y. Two-Dimensional Flower-Shaped Au@Ag Nanoparticle Arrays as Effective SERS Substrates with High Sensitivity and Reproducibility for Detection of Thiram. *J. Mater. Chem. C* **2020**, *8*, 3838–3845.

(5) Wang, K.; Sun, D.-W.; Pu, H.; Wei, Q. Polymer Multilayers Enabled Stable and Flexible Au@Ag Nanoparticle Array for Nondestructive SERS Detection of Pesticide Residues. *Talanta* **2021**, *223*, 121782.

(6) Zhang, L.; Li, X.; Liu, W.; Hao, R.; Jia, H.; Dai, Y.; Usman Amin, M.; You, H.; Li, T.; Fang, J. Highly Active Au NP Microarray Films for Direct SERS Detection. *J. Mater.*

Chem. C **2019**, *7*, 15259–15268.

(7) Tian, H.; Li, H.; Fang, Y. Binary Thiol-Capped Gold Nanoparticle Monolayer Films for Quantitative Surface-Enhanced Raman Scattering Analysis. *ACS Appl. Mater. Interfaces* **2019**, *11*, 16207–16213.

(8) Yan, X.; Wang, M.; Sun, X.; Wang, Y.; Shi, G.; Ma, W.; Hou, P. Sandwich-like Ag@Cu@CW SERS Substrate with Tunable Nanogaps and Component Based on the Plasmonic Nanonodule Structures for Sensitive Detection Crystal Violet and 4-Aminothiophenol. *Appl. Surf. Sci.* **2019**, *479*, 879–886.

(9) Xing, L.; Wang, C.; Cao, Y.; Zhang, J.; Xia, H. Macroscopical Monolayer Films of Ordered Arrays of Gold Nanoparticles as SERS Substrates for in Situ Quantitative Detection in Aqueous Solutions. *Nanoscale* **2021**, *13*, 14925–14934.